

NASA Technical Memorandum 106883
AIAA-95-0300

111-35
44400
11P

Instantaneous 2D Velocity and Temperature Measurements in High Speed Flows Based on Spectrally Resolved Molecular Rayleigh Scattering

Richard G. Seasholtz
*Lewis Research Center
Cleveland, Ohio*

Prepared for the
33rd Aerospace Sciences Meeting and Exhibit
sponsored by the American Institute of Aeronautics and Astronautics
Reno, Nevada, January 9-12, 1995



National Aeronautics and
Space Administration

~~(NASA-TM-106883)~~ INSTANTANECUS 2D
VELOCITY AND TEMPERATURE
MEASUREMENTS IN HIGH SPEED FLOWS
BASED ON SPECTRALLY RESOLVED
MOLECULAR RAYLEIGH SCATTERING
(NASA, Lewis Research Center) 11 p

N95-23461

Unclass

G3/35 0044400



INSTANTANEOUS 2D VELOCITY AND TEMPERATURE MEASUREMENTS IN HIGH SPEED FLOWS BASED ON SPECTRALLY RESOLVED MOLECULAR RAYLEIGH SCATTERING

Richard G. Seasholtz*
NASA Lewis Research Center
Cleveland, Ohio

Abstract

A Rayleigh scattering diagnostic for high speed flows is described for the simultaneous, instantaneous measurement of gas temperature and velocity at a number (up to about one hundred) of locations in a plane illuminated by an injection-seeded, frequency doubled Nd:YAG laser. Molecular Rayleigh scattered light is collected and passed through a planar mirror Fabry-Perot interferometer. The resulting image is analyzed to determine the gas temperature and bulk velocity at each of the regions. The Cramer Rao lower bound for measurement uncertainty is calculated. Experimental data is presented for a free jet and for preliminary measurements in the Lewis 4 inch by 10 inch supersonic wind tunnel.

Introduction

Quantitative techniques for measurement of fluid flow properties in aerospace test facilities are needed to obtain performance data, to validate new computer codes, and to establish facility flow conditions. In many experiments, conventional probe measurements are not adequate because they perturb the flow under study. This is a particularly severe problem in high speed flows in small wind tunnels and in other confined flows such as engine components.

Techniques to measure velocity based on Mie scattering, such as LDV and PIV, require micron size particles to be entrained in the flow. These particles may not always accurately track the flow under study, and thus the velocities obtained may not represent the actual fluid velocity. Particle lag errors can be large when the fluid undergoes high accelerations, as in flows with shocks. Also, in some applications it is either not feasible or not desirable to introduce foreign material into the flow. For example, it is difficult to seed large wind tunnels without contaminating the tunnel. Very high temperature flows, such as in rocket combustion chambers, also make seeding difficult. For these reasons, techniques that are based on molecular scattering are of interest.

A variety of molecular scattering diagnostic techniques have been developed for the measurement of gas density, temperature, and velocity. Included are Rayleigh and spontaneous Raman scattering^{1,2}, laser induced fluorescence³, laser flow tagging⁴, and transient grating spectroscopy⁵.

Rayleigh scattering based diagnostics, the subject of this paper, offer several important features when compared to other molecular scattering methods. Rayleigh scattering is a nonresonant process, so any wavelength laser may be used. This generally means a lower cost, simpler laser system. And, Rayleigh scattering is much stronger (typically by two orders of magnitude) than spontaneous Raman scattering. On the other hand, the resonant processes (such as laser induced fluorescence) generally are much stronger, but they require more complex, more expensive tunable laser systems. Because Rayleigh scattering is not species specific, the gas composition must be known for density and temperature measurements. This, however, is not a factor for an air flow diagnostic, as is being addressed in this paper.

The simplest application of Rayleigh scattering is to measure the total amount of scattered light, which is proportional to the gas density. When the pressure is known, this technique can be used to obtain temperature data. This approach is susceptible to interference from stray laser light and to Mie scattering from particles⁶. (However, use of two wavelengths can be used to reduce the interference from stray laser light⁷.) More information is available from the spectrum of the Rayleigh scattered light. The spectrum is directly related to the velocity distribution of the molecules and thus contains information about the thermodynamic parameters, including temperature and bulk velocity.

The spectral width of Rayleigh scattered light is a result of Doppler broadening caused by the motion of the gas molecules. Since typical molecular speeds are on the order of the speed of sound, the linewidth of the Rayleigh line is only about 1 GHz for air and 90° scattering. A high resolution instrument is thus required to measure the Rayleigh spectrum. Narrow band absorption filters and Michelson and Fabry-Perot interferometers have been used for this work.

Measurement of the Rayleigh scattering spectrum with a scanning Fabry-Perot interferometer has been

* Research Engineer, Optical Measurement Systems Branch

applied to a variety of flow and combustion experiments, such as determining time-average temperature and/or velocity at a point in a hydrogen air flame^{8,9}, in a hydrogen oxygen rocket exhaust plume^{10,11}, and in a wind tunnel test of an ASTVOL model¹².

The Fabry-Perot interferometer has also been used in a static imaging mode (rather than a scanning mode) to measure velocity and temperature in the atmosphere by observing the emission spectrum of atomic oxygen¹³. This imaging method has been used with Rayleigh scattering for one dimensional and planar temperature^{14,15} and velocity measurements¹⁶.

Molecular absorption filters are used for frequency discrimination in the Filtered Rayleigh Scattering technique¹⁷, which was developed to measure density, temperature, and velocity over a planar region. An angularly resolved filtered Rayleigh scattering technique¹⁸ is also being developed for air mass flux measurements and other high speed flow studies.

In this paper, our previously described technique¹⁶ based on a CW laser and Fabry-Perot interferometer to determine time-average velocity in a supersonic free jet over a 2D region is extended to instantaneous measurement of velocity and temperature. The beam from an injection-seeded, frequency doubled Nd:YAG laser is formed into a sheet that illuminates a planar region in the flow. Molecular Rayleigh scattering is collected from the flow and imaged through a planar mirror Fabry-Perot interferometer onto a gated, intensified CCD detector. Analysis of the recorded interference pattern provides estimates of the gas temperature and one component of the velocity at about one hundred localized regions in the imaged area. The use of a pulsed laser for this work allows the determination of the instantaneous velocity field which can be used to calculate turbulence parameters and

spatial correlations. In addition, the pulsed laser permits easy identification of particle images, which can be eliminated in the data processing. An analysis is performed to calculate the Cramer Rao lower bounds for the measurement uncertainties as a function of the flow parameters and the measurement system parameters. Experimental results are presented for a free jet at high subsonic velocities, and some preliminary results are shown for the Lewis 4 inch by 10 inch supersonic wind tunnel.

Theory

Rayleigh scattering

The most basic application of Rayleigh scattering as a diagnostic is to determine gas density by measuring the total amount of Rayleigh scattered light (fig. 1). This does not require resolution of the spectrum.

However, because the Rayleigh scattering cross section is species dependent, the gas composition must be known. If the gas pressure is known, the density can be used to determine temperature. The number of Rayleigh scattering photons N_R collected by an optical system with solid collection angle Ω is

$$N_R = \frac{E_o n L_x \lambda \Omega}{hc} \left(\frac{d\sigma}{d\Omega} \right) \sin^2 \chi \quad (1)$$

where E_o is the laser energy, λ is the wavelength, n the gas number density, L_x the length along the beam of the scattering volume, h Planck's constant, c the velocity of light, $d\sigma/d\Omega$ the differential scattering cross section, and χ the angle between the electric field vector of the (linearly polarized) incident light and the direction of the scattered light. For example, about 500 photons are collected by an $f/8$ optical system from a 1 mm^3 volume of nitrogen at NTP irradiated by a 1 mJ, 532 nm laser pulse.

Resolving the spectrum (fig. 2) of the Rayleigh

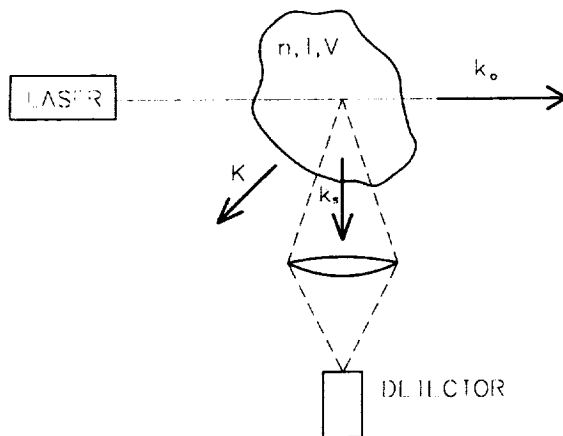


Fig. 1 - Light scattering experiment

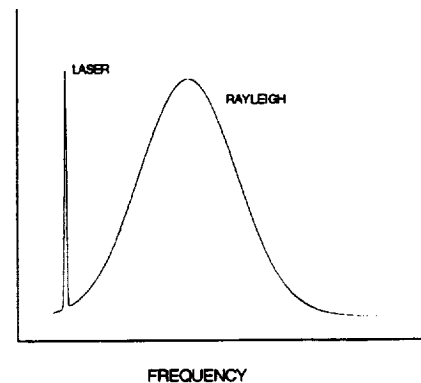


Fig. 2 - Rayleigh scattering spectrum

scattering gives information on gas velocity and temperature. The gas velocity can be determined from the shift in the peak of the spectrum relative to the frequency of the incident laser beam. This shift is proportional to one component of the mean velocity, in a manner analogous to the Doppler shift encountered in laser anemometry. Additional velocity components can be obtained by changing either the direction of the incident beam or the observation direction of the scattered light. Since velocity is determined from only the shift of the spectral peak, this measurement is not affected by the gas composition. Also, scattering from particles entrained in the flow will have a spectral peak at the same location as the Rayleigh scattering peak.

Gas temperature is related to the width of the spectral peak. The shape of the Rayleigh spectrum is a function of the scattering angle and gas density. The simplest example is a single component, low density gas with a Maxwellian velocity distribution. In this case, the scattering occurs independently at each molecule, and the Rayleigh scattering spectrum is a simple Gaussian

$$S(f)df = \frac{1}{\sqrt{\pi} aK} \exp\left\{-\left[\frac{2\pi(f-f_0) - \mathbf{K} \cdot \mathbf{u}}{aK}\right]^2\right\} \quad (2)$$

where, as shown in figure 1, $\mathbf{K} = \mathbf{k}_s - \mathbf{k}_o$ is the interaction wave vector with magnitude (wave number) $K = (4/\lambda)\sin(\theta/2)$, \mathbf{k}_o and \mathbf{k}_s are the wave vectors of the incident and scattered light, θ_s is the scattering angle, $a = (2\kappa T/m)^{1/2}$ is the most probable molecular speed (with κ being Boltzmann's constant, m the molecular mass, T the gas temperature), and \mathbf{u} is the mean gas velocity.

For higher density gases (where the molecular mean free path becomes comparable to or smaller than the scattering interaction wavelength $2\pi/K$), the spectrum is no longer Gaussian in shape. The ratio of the interaction wavelength to the mean free path is

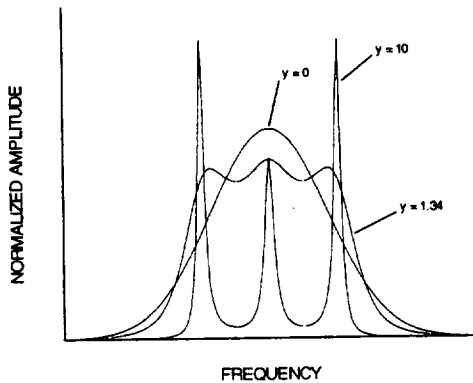


Fig. 3 - Rayleigh scattering spectra for three values of y parameter

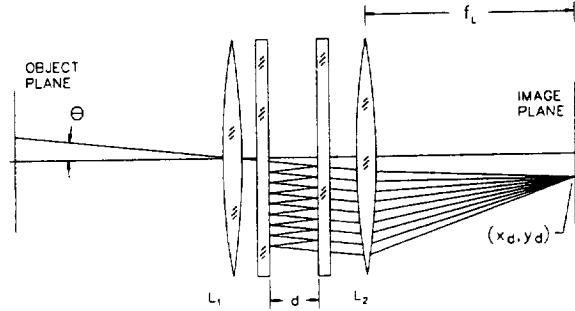


Fig. 4 - Fabry-Perot interferometer

normally expressed as the parameter $y = p/\eta\kappa a$, where p is the gas pressure and η is the shear viscosity. The Gaussian regime (low density) corresponds to $y \ll 1$. For $y \gg 1$ (high density), the scattering spectrum is strongly influenced by collective effects and is characterized by a central peak and two sidebands. The sidebands can be thought of as being caused by scattering from thermally excited acoustic waves. A continuum theory¹⁹ can be used to model the spectrum here. The spectrum in the transition regime, where $y \sim 1$, requires a more detailed kinetic theory. We use the Tenti S6 model²⁰ for this work. Typical spectra for the three regimes are shown in figure 3.

Fabry-Perot interferometer

The Fabry-Perot interferometer (as shown in fig. 4) consists of two partially transmitting planar mirrors. Multiple reflections between the mirrors result in a transmission function (defined as the fraction of light transmitted by Fabry-Perot for a monochromatic source) given by²¹

$$I_{FP}(f, \theta_r) = \left[1 + F \sin^2\left(\frac{2\pi f \mu d_o \cos\theta_r}{c}\right)\right]^{-1} \quad (3)$$

Here, $f=c/\lambda_o$ is the optical frequency, μ is the refractive index of the medium in the Fabry-Perot cavity, d_o is the Fabry-Perot mirror spacing, θ_r is the angle between the ray and the optic axis, and $F = 1/(\sin^2(\pi/2N_E))$ where N_E is the effective finesse. The image of a monochromatic extended source located in the object plane consists of a series of concentric rings, such as shown in figure 8.

Rayleigh spectral measurement using Fabry-Perot interferometer

Consider a laser sheet of energy E_o that uniformly illuminates a region in the object plane (fig. 5). The

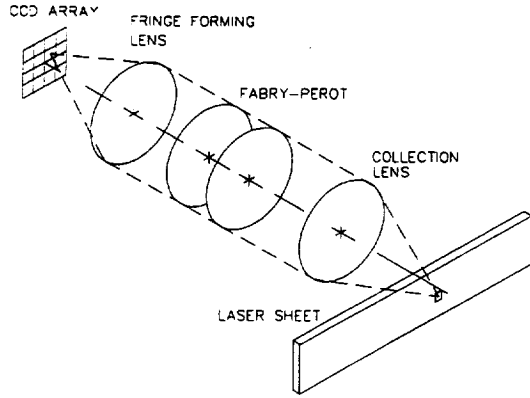


Fig. 5 - 2D scattering experiment using imaging mode Fabry-Perot interferometer

height of the sheet is assumed to be equal to the height of the area viewed by the array detector. The array has N_r rows (measured perpendicular to the beam propagation direction) of square pixels of size L_x by L_x . The expected number of detected photons for the q^{th} pixel can be written

$$\begin{aligned} \langle N_{Dq} \rangle = & \int \int_{\Omega} \int_{\Delta A \rightarrow} [\langle N_{Rq} \rangle S_R(f, \Omega) \\ & + \langle N_{Wq} \rangle \delta(f - f_0)] I(f) df dA d\Omega + B_q \end{aligned} \quad (4)$$

where

$$\langle N_{Rq} \rangle d\Omega = \frac{E_p \epsilon n L_x \lambda_0}{N_r h c M} \left(\frac{d\sigma}{d\Omega} \right) d\Omega \quad (5)$$

is the number of photons scattered (Rayleigh scattering) into solid angle $d\Omega$ that would be detected by the q^{th} pixel if the Fabry-Perot interferometer were not present. Similarly, $\langle N_{Wq} \rangle d\Omega$ is the number of photons due to laser light scattered from windows and walls and is at the laser frequency $f_0 = c/\lambda_0$. Broadband background light, detector dark current, and readout noise are represented by B_q . Although equation 4 does not include scattering from particles, it could be easily incorporated. In equation 5, M is magnification (i.e., size of image of the CCD in the measurement region is $(N_r \times N_c) L_x / M$ where N_c is the number of columns), and ϵ represents the overall detection efficiency (including detector quantum efficiency and system losses). The instrument function $I(f)$ is made up of the Fabry-Perot transmission function $I_{FP}(f)$ and any other filters, such as

a molecular absorption filter. Finally, $S_R(f, \Omega)$ is the spectrum of the Rayleigh scattered light, which is a function of the flow parameters and the optical parameters. The integration over the solid angle is necessary to account for the range of \mathbf{K} vectors over the light collection aperture. For small solid collection angles or low velocities, this effect can be neglected¹⁰ and the integration in equation 4 over Ω can be eliminated. For the work presented here, the effect of aperture broadening was calculated to be on the order 1% or less and was neglected. Spectral broadening can also be caused by sufficiently strong turbulence, but it was not considered in this work. Velocity measurements are not sensitive to aperture broadening since only the frequency of the spectral peak is used, and the spectrum is symmetrically broadened.

Data processing

The Rayleigh scattering images are processed using a nonlinear least-squares fit to a model function represented by equation 4. The y parameter for this flow condition and optical configuration is on the order of one, so the Tenti S6 model is used for calculation of the Rayleigh scattering spectrum. The necessary thermodynamic parameters are calculated using the FLUID program²².

The data reduction procedure is as follows: a number of 30x30 pixel subregions in the recorded image are defined on the fringes (a typical set of subregions is shown in figure 6). A reference image (of elastically scattered laser light) is first analyzed to determine the interferometer finesse and phase of the unshifted laser light at each subregion. (The measured finesse includes the effect of the finite linewidth of the Nd:YAG laser.) The data obtained at the set of subregions are fit to a 2D polynomial. The image of the

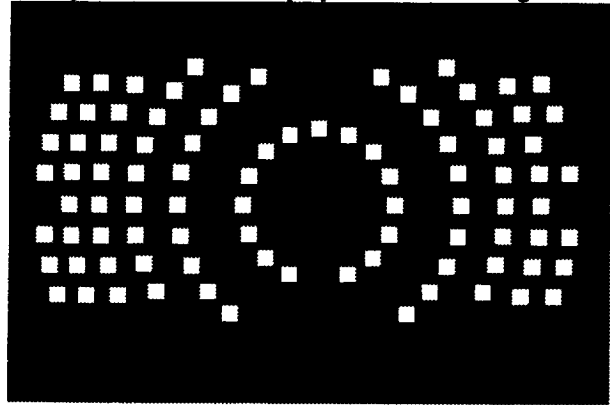


Fig. 6 - Set of subregions used for data processing (actual subregion size is 30x30 pixels, although shown here as 15x15 pixels for clarity).

Rayleigh scattered light is then analyzed at each subregion using the finesse and phase obtained from the reference image. The velocity is calculated from the change of phase and the temperature from the spectral broadening. Another factor that must be accounted for is the broadening caused by the multichannel plate intensifier; the full width half maximum spread of a point source is about 3 pixels. This effect is included by convolving a 2D Gaussian function with the image. As a result of the extensive calculations required for the full evaluation of the model function for the iterative fitting procedure, the time is quite long for the processing an entire image—about 2 minutes on a 90 MHz Pentium PC for each 30x30 pixel subregion. The result of this procedure is a value for the velocity component and the gas temperature at each subregion. For presentation purposes, the sets of velocities and temperatures can be converted to contour plots. It should be reiterated that velocity and temperature data are only obtained for subregions located on the fringes. Data are obtained at a large number of locations, but no data are obtained in the regions between fringes (see fig. 8). To achieve more complete coverage, additional images can be obtained at different Fabry-Perot mirror spacings, which give fringes at different radii. (The data are then not all obtained simultaneously.) In any case, the results obtained with this procedure for each subregion represent average values of velocity and temperature over the subregion. (The size of the subregions for this work are about 0.4 mm square.)

Uncertainty analysis

For light scattering experiments, the uncertainty caused by photon shot noise can readily be evaluated. If this uncertainty is the dominant source of measurement error, as it is in many experiments, then this analysis can be used to estimate the measurement error, and it can be used as a tool for designing the experiment to minimize the error. (On the other hand, if the shot noise induced uncertainty is small compared to other error sources, this analysis comprises only one part of the overall uncertainty analysis.) In any case, the shot noise sets the lower limit for measurement uncertainties. The theoretical least possible uncertainty in the measurements is given by the Cramer Rao lower bound²³. For an ideal spectrum analyzer, the lower bounds for the uncertainty in the density, measured velocity component, and temperature for a Gaussian Rayleigh spectrum are¹⁶

$$\sigma(n) = \frac{n}{\sqrt{N_R}} \tag{6}$$

$$\sigma(V_K) = \frac{a}{\sqrt{2N_R}}$$

$$\sigma(T) = \frac{2T}{\sqrt{2N_R}}$$

where N_R is the total number of detected photons due to Rayleigh scattering (eq. 1 or eq. 5). Stray laser light and background noise are neglected.

As an example, consider nitrogen at NTP ($T=293$ K, $p = 1$ atm., $n = 2.5 \times 10^{25} \text{ m}^{-3}$), a single 1 J pulse from a 532 nm laser, $d\sigma/d\Omega = 6.1 \times 10^{-32} \text{ m}^2/\text{sr}$, an array detector having 384 rows of 23 μm square pixels, a 1:1 imaging system having $f/8$ collection optics ($\Omega = 0.0123$ sr), and a 1% overall detection efficiency. Using equation 5, the expected number of detected photons from a single pixel area is $\langle N_{Rq} \rangle = 30$. Thus, for a 30x30 pixel region, the number of expected counts would be 27,000, and the lower bounds on the precision of density, temperature, and velocity measurements are 0.6 %, 2.5 K, and 1.8 m/sec, respectively. It must be emphasized that these uncertainties are based on the assumption of ideal spectrum analysis. Actual measurements based on some type of interferometer or absorption medium will, of course, have a higher lower bound for the uncertainties. It was previously shown¹⁶ that for the case of no wall scatter, the lower bound for the Fabry-Perot based system is about a factor of 5

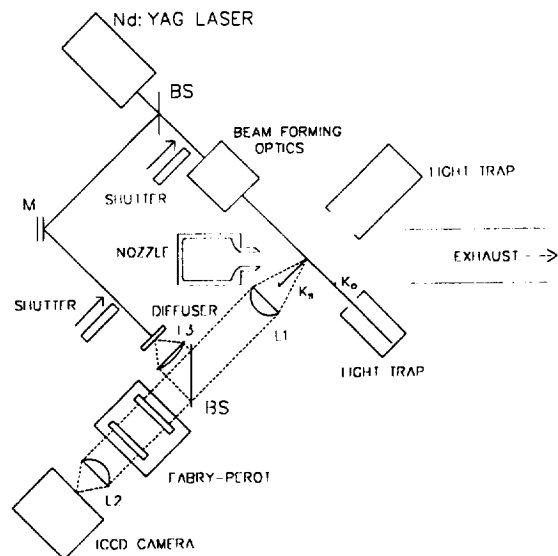


Fig. 7 - Optical setup for measuring axial velocity component in free jet

larger than for an ideal spectrum analyzer for velocity and about a factor of 10 larger for temperature.

Experiments

Free jet

Initial laboratory measurements were made in a small free jet to validate the technique (fig. 7). The exit diameter was 9.5 mm. The air supply to the nozzle was filtered to remove particulates with diameters larger than 0.2 μm . The beam from an injection seeded, frequency doubled, Nd:YAG laser with 0.9 J pulse energy was formed into a sheet that crossed the flow at 45° as shown in the figure. The sheet thickness was about 0.2 mm and the height was about 7 mm. A commercially available Fabry-Perot interferometer was used. The mirrors (70 mm diameter, $\lambda/200$ flatness, and 90% reflectivity) were set at a 14.96 mm spacing for the measurements reported here, which corresponded to free spectral range (FSR) of about 10 GHz. Rayleigh scattered light was collected and collimated with lens L1 (250 mm focal length lens). The scattering angle was 90°. After passing through the pellicle beam splitter and Fabry-Perot interferometer, the light was



Fig. 8 - Reference image for first free jet image



Fig. 9 - First Rayleigh scattering image for free jet; note particle images in upper right

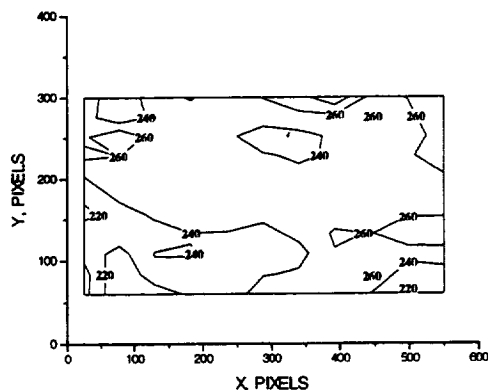


Fig. 10 - Velocity contour plot for first free jet image; contours in m/sec

focused onto the detector (multichannel plate intensified, cooled CCD array with 576x384 23 μm square pixels) by lens L2 (300 mm focal length 35 mm camera lens with 1.4X teleconverter). The images digitized with a 14 bit A/D converter and transferred to a laboratory computer for storage and analysis.

A beamsplitter was used to direct a small amount of light from the laser onto an opal glass diffuser to serve as a reference image. A condenser lens collimated the light from the diffuser, which was then directed into the Fabry-Perot by an uncoated pellicle. Remotely controlled shutters were used to block either the main beam (for recording the reference image) or the reference beam (for recording the Rayleigh image).

The measurement plane was intersected by the jet axis 12 mm downstream from the nozzle exit plane. Data for a single flow condition are presented here; the axial velocity and static temperature calculated from the isentropic flow equations were 255 m/sec and 280 K. Three representative images are shown. Each was taken with a single laser pulse. The Fabry-Perot mirror spacing was different for the three images, so the fringes are at different radii. The first Rayleigh image along with its associated reference image are shown in figures 8 and 9. This image was analyzed at the 90 subregions shown in fig. 6. The flow direction was assumed to be along the jet axis for the purpose of converting the measured velocity component (which is along **K**) to the velocity magnitude. The y parameter was about 0.9, so the Tenti S6 model for the Rayleigh spectrum was used. Velocity data were converted to the contour plot shown figure 10. The velocity measurements near the center of the image were close to the isentropic flow values. Temperature data are not shown for this image because of inadequate detector resolution at the outer fringes.

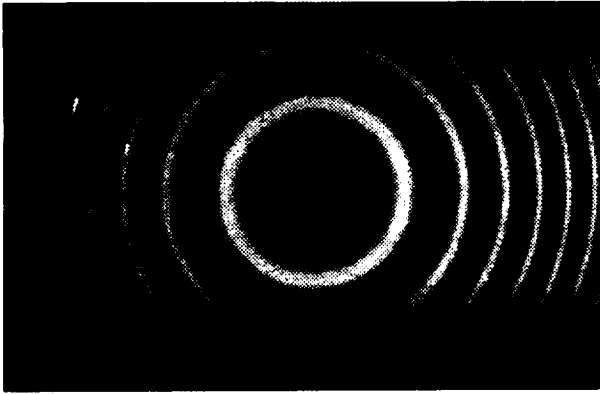


Fig. 11 - Second free jet Rayleigh scattering image

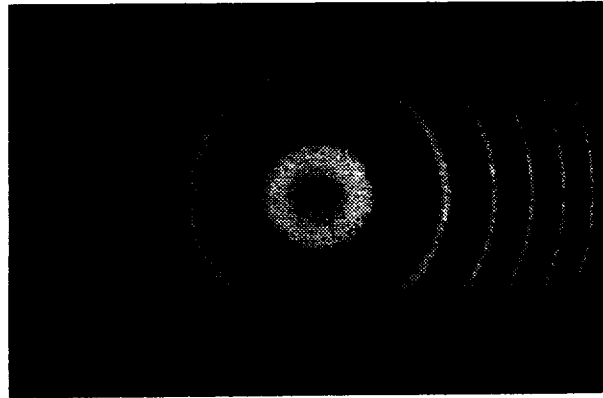


Fig. 13 - Third free jet Rayleigh scattering image

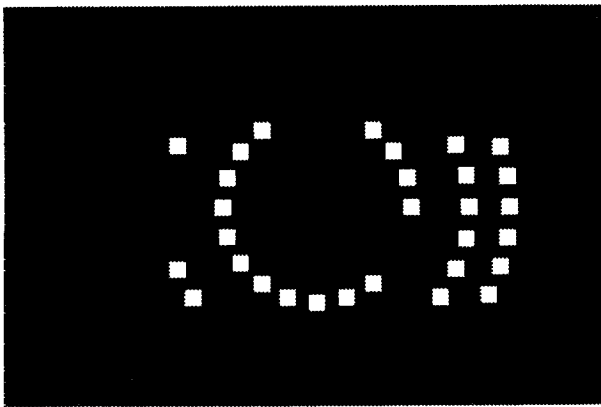


Fig. 12 - Subregions analyzed for second free jet image (fig. 11)

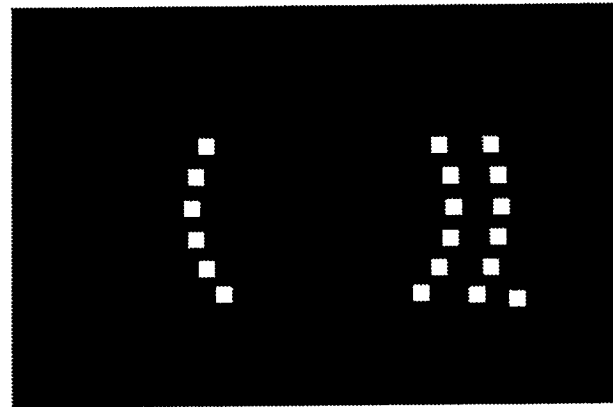


Fig. 14 - Subregion analyzed for third free jet image (fig. 13)

The second and third Rayleigh images were analyzed at a smaller number of subregions located on the inner fringes. The second image was analyzed at 30 subregions (fig. 11). The mean velocity was 250 m/sec, with standard deviation of 11 m/sec. The mean temperature was 270 K, with standard deviation of 23 K.

The third image was analyzed at 19 subregions (fig. 12). The mean velocity was 252 m/sec, with standard deviation of 11 m/sec. The mean temperature was 267 K, with standard deviation of 16 K.

For this optical geometry and flow, the Cramer Rao lower bounds (for an ideal spectrum analyzer) for velocity and temperature were about 0.4 m/sec and 0.6 K. The measurement precision based on the observed variance in the data for the second and third images was about 10 m/sec and 20 K. The variance was greater for the first image with more subregions covering a larger part of the image field. The might be caused by the limited spatial resolution of the intensified CCD. Good agreement between the measured mean velocity and the velocity calculated from the isentropic flow equations.

However, the mean measured temperature was significantly less than the isentropic temperature, particularly in the first image with 90 subregions where it was 50 K low. The the other two images, with fewer subregions, were low by about 10 K. Note that no adjustable parameters were used in obtaining these velocities and temperatures. Measurements of a known temperature gas could be used to obtain calibration parameters that could be used to increase the accuracy of the temperature measurements.

Supersonic wind tunnel

The Rayleigh scattering system was recently installed in the Lewis 4 inch by 10 inch supersonic wind tunnel, and some preliminary data were obtained. The optical system was identical to the layout described in the above section for the free jet measurements, except for the optics used to introduce the beam into the tunnel. The tunnel was equipped with a Mach 2 nozzle, and the air supply was passed through a 0.2 μm filter to remove particles. For the first tests, the laser beam was transmitted through a window into the plenum chamber

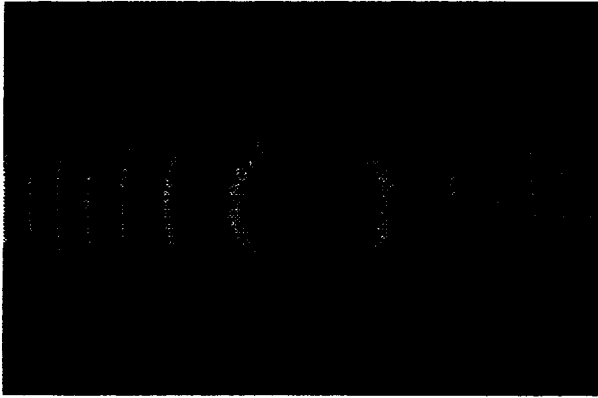


Fig. 15 - Rayleigh scattering image for supersonic wind tunnel

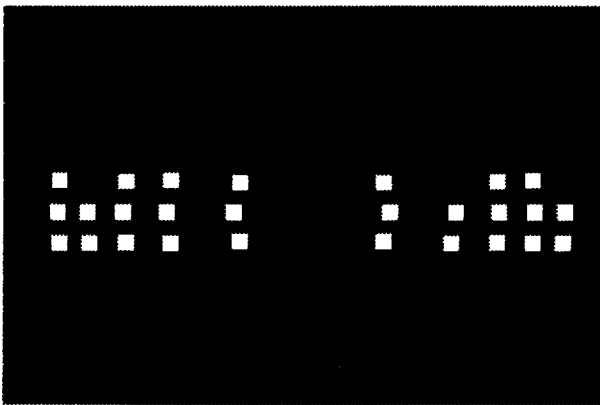


Fig. 16 - Subregions (27) analyzed for supersonic wind tunnel image

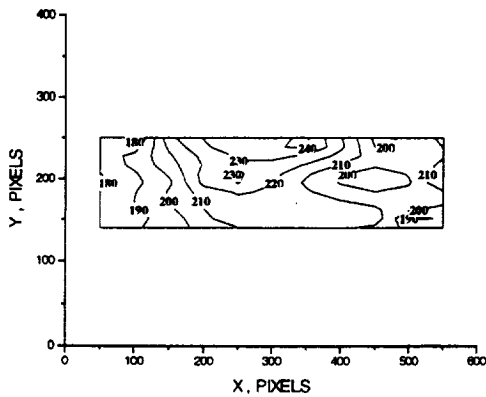


Fig. 17 - Temperature contours for supersonic wind tunnel (fig. 15)

and propagated downstream through the nozzle and the test region. Light scattered at 90° was collected through a window in the tunnel sidewall. A typical fringe pattern (for a single laser pulse) is shown in figure 15.

For this measurement, the laser beam was focused to about 2 mm diameter. As can be seen in the image, the amount of stray laser light detected was small, and the filter effectively removed particles in the air supply.

One problem in this test environment was the high level of acoustic noise, which caused vibration of the optics. This resulted in shot-to-shot variation in the phase of the reference images. As a result of this variation, the velocity could not be obtained from the phase shift between subsequent reference and Rayleigh images. Instead, a value for the reference phase was obtained from a part of the Rayleigh image dominated by stray, unshifted laser light (e.g., near the bottom of the image in fig. 13). Temperature data, since they are obtained from the broadening rather than the location of the spectral peaks, are not as sensitive to the shot-to-shot phase variation. A temperature contour plot based on 27 subregions (fig. 16) is shown in figure 17. The mean measured temperature was 202 K with a standard deviation of 23 K. The estimated velocity was 390 m/sec, which correspond to about Mach 1.4 flow based on isentropic flow from the plenum. Acoustic shielding material will be used in future test to isolate the laser and optics. Another approach, which was used for these preliminary measurements, would be to obtain the reference frequency information from the same image used for the Rayleigh light.

Concluding Remarks

Molecular Rayleigh scattering measurements made in a free jet and in a small supersonic wind tunnel demonstrated the feasibility of using an injection-seeded Nd:YAG laser and Fabry-Perot interferometer to obtain a large number (on the order of one hundred) simultaneous, instantaneous measurements of gas temperature and velocity in a planar region of flow fields. Good agreement was obtained in free jet measurements for both temperature and velocity. Several issues, however, must be addressed in the application of this technique in the harsh environment of test facilities.

Stray laser scattering must be carefully controlled. In many experiments the stray laser light can be managed with apertures and light traps. In high speed flows (supersonic), where the spectrum is shifted from the laser frequency, a molecular absorption filter can be used to reject the stray light. In addition, the laser and the Fabry-Perot interferometer must be isolated from high noise levels. This can be done with acoustic shielding and vibration isolation equipment, or the laser and interferometer can be remotely located and the light transmitted through relay optics or optical fibers.

Acknowledgments

We would like to acknowledge the efforts of Mr. W. Trevor John, who was responsible for setting up and aligning the optical system used for this work. Also, Prof. G. Tenti kindly provided us with the computer code for his 6 moment Rayleigh scattering model. And, Mr. Alvin Buggele graciously provided us access to the 4 inch by 10 inch supersonic wind tunnel.

References

- ¹ N.M. Laurendeau, "Temperature measurements by light-scattering methods", *Developments in Experimental Techniques in Heat Transfer and Combustion: Proceedings of the 24th National Heat Transfer Conference*, Pittsburgh, Aug. 9-12, 1987.
- ² A.C. Eckbreth, "Laser Diagnostics for Combustion, Temperature, and Species", Abacus Press, Tunbridge Wells, Kent, 1988.
- ³ M. Allen et al., "Velocity field imaging in supersonic reacting flows near atmospheric pressure", *AIAA J.*, **32**, pp. 1676-1682, 1994.
- ⁴ R.B. Miles et al., "Instantaneous profiles and turbulence statistics of supersonic free shear layers by Raman excitation plus laser-induced electronic fluorescence (Relief) velocity tagging of oxygen", *Exp. Fluids*, **8**, pp. 17-24, 1989.
- ⁵ M. Brown, P. DeBarber, J. Maggart, and R. Pitz, "Measurements of NO_x Using Transient Grating Spectroscopy", *AIAA 33rd Aerospace Sciences Meeting*, Reno, AIAA paper 95-0425, 1995.
- ⁶ B. Shirinzadeh, M.E. Hillard, and R.J. Exton, "Condensation effects on Rayleigh scattering measurements in a supersonic wind tunnel", *AIAA J.*, **29**, pp. 242-246, 1991.
- ⁷ M.V. Otugen, K. Annen, and R.G. Seasholtz, "Gas temperature measurements using a dual-line detection Rayleigh scattering technique", *AIAA Journal*, **31**, pp. 2098-2104, 1993.
- ⁸ R. Cattolica, F. Robben, and L. Talbot, "The interpretation of the spectral structure of Rayleigh scattered light from combustion gases", *AIAA 14th Aerospace Sciences Meeting*, Washington, AIAA paper 76-31, 1976.
- ⁹ R.W. Pitz, et al., "Temperature and density in a hydrogen air flame from Rayleigh scattering", *Comb. and Flame*, **27**, pp. 313-320, 1976.
- ¹⁰ R.G. Seasholtz, F.J. Zupanc, and S.J. Schneider, "Spectrally resolved Rayleigh scattering diagnostic for hydrogen oxygen rocket plume studies", *Journal of Propulsion and Power*, **8**, pp. 935-942, 1992.
- ¹¹ F.J. Zupanc and J.M. Weiss, "Rocket plume flowfield characteristics using laser Rayleigh scattering", *AIAA/SAE/ASME/ASME 28th Joint Propulsion Conference*, Nashville, July 6-8, AIAA paper 92-3351, 1992.
- ¹² H.E. Kourous and R.G. Seasholtz, "Fabry Perot interferometer measurement of static temperature and velocity for ASTOVL model tests", *ASME Symposium on Laser Anemometry: Advances and Applications*, Lake Tahoe, 1994.
- ¹³ G.G. Sivjee, T.J. Hallinan, and G.R. Swenson, "Fabry Perot interferometer imaging system for thermospheric temperature and wind measurements", *Appl. Opt.*, **19**, pp. 2206-2209, 1980.
- ¹⁴ J.L. Lock, R.G. Seasholtz, and W.T. John, "Using Rayleigh Brillouin scattering to determine one dimensional temperature and number density profiles of a gas flow field", *Appl. Opt.*, **31**, pp. 2839- 2848, 1992.
- ¹⁵ R.G. Seasholtz and J.A. Lock, "Gas temperature and density measurements based on spectrally resolved Rayleigh-Brillouin scattering", *NASA Langley Measurement Technology Conference*, Hampton, VA, 1992.
- ¹⁶ R.G. Seasholtz, "2D Velocity and Temperature Measurements in High Speed Flows based on Spectrally Resolved Rayleigh Scattering", *New Trends in Instrumentation for Hypersonic Research*, A. Boutier (ed.), Kluwer Academic Publishers, Boston (1993).
- ¹⁷ R.B. Miles, W.R. Lempert, and J. Forkey, "Instantaneous velocity fields and background suppression by filtered Rayleigh scattering", *AIAA 29th Aerospace Sciences Meeting*, Reno, AIAA paper 91-0357.
- ¹⁸ J.A. Shirley and M. Winter, "Air mass flux measurement system using Doppler Shifted filtered Rayleigh scattering", *AIAA 31st Aerospace Sciences Meeting*, Reno, AIAA paper 93-0513, 1993.
- ¹⁹ N.A. Clark, "Inelastic light scattering from density fluctuations in dilute gases. The kinetic hydrodynamic transition in monatomic gas", *Phys. Rev. A*, **12**, 232-244, 1975.
- ²⁰ G. Tenti, C.D. Boley, and R.C. Desai, "On the kinetic model description of Rayleigh Brillouin scattering from molecular gases", *Can. J. Phys.*, **52**, pp. 285-290, 1974.
- ²¹ J.M. Vaughan, "The Fabry Perot Interferometer. History, Theory, Practice and Applications", Adam Hilger, Bristol, Chapter 3, 1989.
- ²² T.E. Fessler, "FLUID: A Numerical Interpolation Procedure for Obtaining Thermodynamic and Transport Properties of Fluids", *NASA TM X-3572*, 1977.
- ²³ A.D. Whalen, "Detection of Signals in Noise", Academic Press, New York, pp. 324-331, 1971.

REPORT DOCUMENTATION PAGE

Form Approved
OMB No. 0704-0188

Public reporting burden for this collection of information is estimated to average 1 hour per response, including the time for reviewing instructions, searching existing data sources, gathering and maintaining the data needed, and completing and reviewing the collection of information. Send comments regarding this burden estimate or any other aspect of this collection of information, including suggestions for reducing this burden, to Washington Headquarters Services, Directorate for Information Operations and Reports, 1215 Jefferson Davis Highway, Suite 1204, Arlington, VA 22202-4302, and to the Office of Management and Budget, Paperwork Reduction Project (0704-0188), Washington, DC 20503.

1. AGENCY USE ONLY (Leave blank)		2. REPORT DATE March 1995	3. REPORT TYPE AND DATES COVERED Technical Memorandum	
4. TITLE AND SUBTITLE Instantaneous 2D Velocity and Temperature Measurements in High Speed Flows Based on Spectrally Resolved Molecular Rayleigh Scattering			5. FUNDING NUMBERS WU-505-62-50	
6. AUTHOR(S) Richard G. Seasholtz				
7. PERFORMING ORGANIZATION NAME(S) AND ADDRESS(ES) National Aeronautics and Space Administration Lewis Research Center Cleveland, Ohio 44135-3191			8. PERFORMING ORGANIZATION REPORT NUMBER E-9481	
9. SPONSORING/MONITORING AGENCY NAME(S) AND ADDRESS(ES) National Aeronautics and Space Administration Washington, D.C. 20546-0001			10. SPONSORING/MONITORING AGENCY REPORT NUMBER NASA TM-106883 AIAA-95-0300	
11. SUPPLEMENTARY NOTES Prepared for the 33rd Aerospace Sciences Meeting and Exhibit sponsored by the American Institute of Aeronautics and Astronautics, Reno, Nevada, January 9-12, 1995. Responsible person, Richard G. Seasholtz, organization code 2520, (216) 433-3754.				
12a. DISTRIBUTION/AVAILABILITY STATEMENT Unclassified - Unlimited Subject Category 35 This publication is available from the NASA Center for Aerospace Information, (301) 621-0390.			12b. DISTRIBUTION CODE	
13. ABSTRACT (Maximum 200 words) A Rayleigh scattering diagnostic for high speed flows is described for the simultaneous, instantaneous measurement of gas temperature and velocity at a number (up to about one hundred) of locations in a plane illuminated by an injection-seeded, frequency doubled Nd:YAG laser. Molecular Rayleigh scattered light is collected and passed through a planar mirror Fabry-Perot interferometer. The resulting image is analyzed to determine the gas temperature and bulk velocity at each of the regions. The Cramer Rao lower bound for measurement uncertainty is calculated. Experimental data is presented for a free jet and for preliminary measurements in the Lewis 4 inch by 10 inch supersonic wind tunnel.				
14. SUBJECT TERMS Rayleigh scattering; Fabry-Perot interferometers			15. NUMBER OF PAGES 11	
			16. PRICE CODE A03	
17. SECURITY CLASSIFICATION OF REPORT Unclassified	18. SECURITY CLASSIFICATION OF THIS PAGE Unclassified	19. SECURITY CLASSIFICATION OF ABSTRACT Unclassified	20. LIMITATION OF ABSTRACT	